Strategy and criteria to optically design a solar concentration plant

D. Jafrancesco, P. Sansoni *, F. Francini, D. Fontani

CNR-INO National Institute of Optics, Largo E. Fermi, 6, Firenze, 50125, Italy

ARTICLE INFO

ABSTRACT

The objective of this work is to individuate the best strategy to determine the layout of a thermodynamic plant based on the concentration of solar flux by means of a large number of mirrors. Many software tools exist, both dedicated software and more general optical software. This analysis shows the advantages derived from the use of a general non-sequential optical software, proposing criteria and procedures in order to establish dedicated optical merit figures, which are suggested and evaluated from the point of view of their effectiveness to achieve a favorable layout design. Particular attention is devoted to merit figures that estimate the optical efficiency, a key quantity for all the CSP plants that can be defined in different ways. The description includes examples of application, discussion of results and various proposed alternatives for the merit figure.

Contents

1. Introduction

Recently the sector of production of renewable energy is experiencing a great development of systems based on the concentration of solar flux by means of a large number of mirrors. These Concentrated Solar Power (CSP) plants are thermodynamic solar energy installations that are mainly composed of a field of heliostats, which concentrate the sunlight on a receiver, often placed on a tower.

In order to maximize the system efficiency, the utilization of suitable optical design software to structure the mirror field and the receiver is indispensable. At present for CSP systems it is possible to utilize different codes and software tools in order to evaluate the optical performances of the mirror field [1] and to simulate the flux distribution on the inner surfaces of cavity or receiver, which is practically impossible to get by real measurements (for example, see Qiang Yu et al. in [2]). They permit to obtain several merit figures, many of them introduced and employed in literature, in order to evaluate the performance of a whole renewable energy plant: as example, [3] proposes "net energy" and "gross carbon emission (CO2eq)" as merit figures in order to compare different sources for electricity generation, while [4] utilizes "embodied energy", devoted to total cost evaluation (it considers only commercial energy) and "emergy", that is the amount of energy involved in a transformation process. Scholars

* Corresponding author. Tel.: +39 055 23081; fax. +39 055 2337755.
E-mail address: paola.sansoni@ino.it (P. Sansoni).

introduced different merit figures to evaluate costs and advantages of the sources for energy generation (in particular, to compare their results in terms of efficiency, costs, sustainability and environmental protection), but very often they are general figures that do not specifically characterize the optical configuration of the heliostat field. In effect, problems and methods related to the heliostat plant realization suggested to use appropriate merit figures to characterize the CSP optical system and to guide the design process, as it was done for other solar systems or components. Kumar, in [5], estimates the design parameters for a box-type solar cooker introducing two merit figures related to heat losses and water heating capability; Sansoni et al., in [6], investigate the image uniformity separating the contributions of different regions of a prismatic lens, while in [7] carefully analyze the performance of a simulated trough collector, assessing by ray-tracing received light and acceptance angle. All these papers evidence the necessity of introducing some merit figures specific for the actual case. From this point of view, the utilization of a generic optical design software permits more flexibility to individuate the actual best merit figures and to assess the performances concerning flux distribution and system collection efficiency with respect to dedicated software (see [1] for a review of specific codes for solar flux calculation). Obviously, the utilization of a generic optical design software requires the development of customized methods and design tools, as studied by Sansoni et al. in [8], but it permits to choose the best evaluation tools. Very interesting is the work of Segal et al., in [9–11], where the optimization is focused on the maximization of the energy at the entrance of the receiver system in a tower-reflector system. It is essential to highlight that the traditional merit figures for optical systems are quite useless, because solar divergence and component tolerances very often generate a beam enlargement wider with respect to the optical aberrations. Moreover, the optical aberrations exist only if the solar field is composed of non-flat mirrors: in this case the actual most important aberration, the astigmatism, can be significantly reduced if a suitable plant layout is utilized; coma and spherical aberration, for large solar plants, are often unimportant [12,13]. For this reason the best choice is a non-sequential optical design software (like ASAP, LighTools, TracePro), from which it is possible to obtain more useful information with respect to a traditional (sequential) one. Basically, optical design software tools can be split into two categories: traditional software, where the user decides the order in which the rays hit the surfaces; lighting simulation software, where the rays hit the surfaces in a "natural" order, depending on their optical path (more similar to the physical reality). A sequential software permits to calculate the aberration values, while the non-sequential ones focus on radiometric and photometric quantities: the most useful of them, for the analysis of the performances of a mirror field, are the irradiance maps that show both "how much" (scalar quantities, i.e. the total flux on the surface) and "how" (imaging maps, i.e. the flux distribution) of the ray tracing.

The present paper is dedicated to summarize the merit figures utilized for the design of CSP plants using a generic optical design software, separating the subsystems [9] and focusing on methods and tools to evaluate the optical performance of a heliostat field in order to choose the best plant configuration.

2. Field of heliostats

The first phase of the optical design of a CSP plant is to define the field of mirrors, thus a set of parameters that permit to evaluate and classify it, from an optical point of view, must be outlined. Defined the plant location [14], the positions where the heliostats have to be placed are determined by the mirror size and the

acceptability of a shadowing degree and a blocking grade in various day hours/seasons. The degree of shadowing is how much a mirror's shadow can cover the mirror behind; the grade of blocking defines how many rays from a heliostat to the receiver are blocked by the rear surface of other mirrors. Many tools and procedures developed by means of a non-sequential optical software can be utilized in this phase in several ways: shadowing and blocking phenomena can be evaluated in different day hours or seasons in order to establish a convenient trade-off between land occupation and CSP plant efficiency; the land occupation is computable also by a reverse ray-tracing from the receiver toward the mirror field, measuring the flux not intercepted by the heliostats. Many authors studied the influence of these parameters on the final optical efficiency of a CSP system [15–19], but the real difficulty is to find a useful merit figure to compare different mirror fields or the same heliostat field in different hours of the day or seasons. In fact the actual input flux depends on the system configuration: it varies with the cosine factor and the mirror shadowing factor. Thus the efficiency (output flux / input flux) based on the actual input flux is not very useful to compare different layouts of the same field (for example with towers of different height), because an increase of the shadowing (that is a decrease of the input flux) and a proportionally identical decrease of the output flux lead paradoxically to the same efficiency. Jafrancesco et al., in [20], defined a new merit figure that describes the field collection efficiency: it is the ratio between a variable *field output flux* (quantity of radiation reflected by the mirror field towards the receiver) and a constant *field input flux*, defined as the product between the DNI and the total reflecting surface, where the DNI is the *Direct Normal Insolation*. Substantially this is a conventional definition of mirror field efficiency, where the actual input flux is replaced by the so-defined *field input flux*, and it is always less than 1. This definition could be useful to compare different fields layouts (setting the actual sun position), but it does not take into account the cosine factor (that is the angle between the normal to the mirror surface and the sun rays). In effect, it has to be highlighted that it is mandatory to individuate the "critical parameters" concerning the realization of a CSP plant, as the area of the mirroring surface or the land occupation. If the last one is the major concern, it seems preferable to use as input flux the product of DNI and area utilized by the CSP plant[1] (obviously only to compare CSP plants with different mirroring surface, because for the same plant the merit figure introduced in [20] is equivalent); moreover, the averaged cosine factor can be evaluated and considered in the formulas in order to estimate the flux that hits the mirroring surface without blocking.

Regarding two-dimensional (2-D) and three-dimensional (3-D) maps that represent the distribution of the parameters of interest (e.g. irradiance, shadowing, output flux, …), they are the output of a software simulation and act both as qualitative figure and as "parameters set". So from them it is possible to obtain various merit figures; in fact a quantitative measurement of the performance requires the passage from a 2-D or a 3-D map to unidimensional parameters (just because there is no ordering among the 2-D or 3-D maps, thus it is impossible a quantitative comparison between two configurations of CSP plant). However, the qualitative analysis of the performance is very useful in order to warn the designer about some weaknesses or faults in the CSP layout that are very difficult to be obtained from consolidated data: they typically are lack of irradiance or efficiency of a part of

---

[1] Please note that it would be possible to define a more general merit figure too: the ratio between the averaged (annual) output flux from the mirror field and the area of CSP plant; it would seem to permit for comparison among CSP plants in different locations, which is really very difficult due to the design priority change (land occupation, area of the mirroring surface, limits to tower height, etc.).

the CSP plant. An exception is represented by the irradiance maps on the receiver surface, which could be directly utilized as input for a thermal analysis software.

In this perspective, a non-sequential optical software owns the capability to calculate maps and data judged more useful during the design phase, even if the calculus was not previously considered.

3. Secondary optics

Also for the analysis of the secondary optics, a non-sequential optical design software can be the best choice, because it permits to analyze more effectively the behavior of the secondary optics. In fact, several plant layouts (in particular concerning solar furnaces) include the utilization of another optical component (in addition to the heliostats) to improve the concentration on the receiver. This component can be another mirror set, a faceted mirror or a concentration stage, like a CPC (Compound Parabolic Concentrator) [21].

Generally, the most important merit figure, for the secondary optics, is its optical efficiency, which is clearly definable as the ratio between output flux and input flux. This ratio depends only on layout and characteristics of the secondary optics, and it can be used also for further optical systems that could be present. However, depending on the configuration, there are other merit figures that can be exploited. Indeed, due to the large variety of secondary optics, the optical analysis has to be compliant to the specific kind of layout. An example of that is the evaluation of the CPC efficiency. Various authors studied different merit figures in order to characterize the CPCs [22,23], but they neglected the quantity of radiation that directly exits from the output window of the CPC. This radiation has an influence not only on the CPC efficiency [24], but also on the need of using a cooling system for the CPC surface. In practice, the CPC surface has a reflectivity value of about 85–95% (it depends on the presence of a surface coating and its ageing) and the energy absorbed by its surfaces causes both a decrease of the flux at the CPC output window and an increase of the CPC temperature. Therefore, it is useful to know the fraction of the input flux that directly exits from the output window, defined as *direct fraction of the CPC*. This value, that is equivalent to the ratio between output flux and input flux when the CPC surfaces are perfect absorbers, can be easily assessed by means of simulation software and codes, which permit to change the surface characteristics of all the optical components.

This example clearly shows that the purpose of setting a suitable merit figure is to permit a comparison among different optical layouts under many point of views: in the mentioned case, it is interesting not only the flux decrease due to the imperfect reflectance of the CPC internal surface, but also the temperature boost of the last one.

4. Receiver

The ultimate aim of the optical designer that deals with a mirror field is to obtain on the receiver the established irradiance distribution [25]. The receiver can be represented by the internal walls of a cavity, a set of tubes or an absorbing surface. However, there is an input window (coincident with the receiver if this is an absorbing surface) where the entering flux is evaluated, eventually by means of an irradiance map on the input window (regarded as a virtual surface); other irradiance maps of the absorbed flux on the cavity walls allow calculating the local thermal exchange with the fluid system.

Depending on the utilized optical design software, the available flux (input flux minus reflected flux)[2] can be calculated in different ways: for example, in Lambda Research TracePro, in the irradiance map of the input window, the reflected flux (exiting from the cavity) is added to the true input flux because the software does not take into account the algebraic sign of the flux. Then, in order to calculate the available flux it is necessary to separately evaluate the "(input+reflected) flux" and the true input flux (this latter can be calculated setting all cavity walls as perfect absorbers). Thus, available flux=2 · input flux − (input+reflected) flux. In any case, the knowledge of the available flux and the evaluation of the other losses permit to calculate the expected values of useful flux (for example the flux transferred to the thermal medium, molten salt or other types) and to correctly calculate the receiver size, as Steinfed and Schubnell in [27].

From the irradiance distribution on the input window of the receiver, it is possible to extract some data:

– the total flux that hits the input window;
– the max/min irradiance ratio (*uniformity*);
– the *marginal irradiance*.

The first parameter is a standard datum and it does not need further explanations; concerning the uniformity, this value is relevant if the input window coincides with the absorbing wall, because it gives indications about its thermal stressing. Obviously, if the receiver is a cavity the uniformity has to be calculated on the cavity walls; in any case there is a strong dependence of uniformity on the calculation method, in particular the smoothing on the irradiance map heavily affects the uniformity. Interesting is also the marginal irradiance, another example of a parameter, obtained by a non-sequential software, that could be useful only in some cases and deserves some describing details. The marginal irradiance was introduced from Jafrancesco et al. in [20] as the irradiance on the border limit, averaged on a narrow ring at the edge of the receiver. It measures the flux amount approximately lost or gained if the receiver is slightly restricted or enlarged (if the examined receiver is a cavity, the study has to refer to its input window). The utility of the marginal irradiance is based on the fact that the phenomena related to the receiver losses are highly dependent on the receiver area: for example, if this area is increased it is possible to evaluate if the gain about the collecting flux exceeds the losses due to Planckian radiation and wind effect.[3] Moreover, very often the irradiance profile on the receiver (or input window) shows a Gaussian shape, mainly due to mechanical tolerances, pointing errors and mirror surface defects [28–30]; in this case the ratio between marginal irradiance and maximum irradiance easily marks the shape of the irradiance plot, ultimately the fraction of flux that enters into the receiver. Truly all the information is contained in an irradiance plot on a plane coincident with the input window of the receiver, but they are not directly comparable in order to evaluate the best configuration without extrapolating one or more parameters. Then, the marginal

---

[2] Conductive, convective and Planckian losses cannot be estimated by means of an optical design software, then the available flux is not equal to the flux transferred to the fluid; the reflection losses, on the contrary, can be correctly evaluated because they depend only on the reflectance of the receiver wall and on the receiver shape [26].

[3] Really the flux on the input window is very often the datum that marks the passage between optical and thermal merit figures: the thermal designer of the CSP plant has to set the minimum and optimum flux transferred to the fluid; if there is an analytical or numeric evaluation of the losses variation depending on the input window dimension, the comparison between marginal irradiance and "marginal exitance" (due to all flux losses depending on the input window dimension) could be a key analysis.

irradiance is a parameter (like total flux or mean irradiance) that permits this comparison.

Another example of extrapolation of information from two-dimensional maps is the *isocandela plot* of the rays reflected by the mirrors, which permits to correctly orientate the receiver. The isocandela plot shows the direction of rays on the internal surface of a hemisphere placed at the infinity (the axis of the hemisphere is set by the user); it is a very intuitive representation of the angular distribution of the radiation. The parameter to be extracted, in this case, is the difference between direction of the radiation from the mirror field and orientation of the axis of the receiver; if there is a secondary optics as a CPC, this parameter affects the direct fraction of the CPC, influencing both the flux entering into the receiver and the quantity of heat that the CPC must dissipate.

5. Tests on a simulated solar field

5.1. Simulated layout

This section is dedicated to test some parameters introduced as examples in the previous paragraphs; these tests are performed referring to a simulated CSP plant; its heliostat field was realized as a set of 186 spherical mirrors (with circular shape, radius 1 m, height of mirror center from the ground 1.5 m), arranged in rows and columns: the distance between two adjacent mirrors of the same row is 3 m and the spacing between rows is 2.5 m. Setting a reference system with Z axis in vertical direction, Y axis in the North-South direction and X axis in the East-West direction (with the origin on the ground), the first row has $Y = -20$ m, the last one $Y = 47.5$ m; the heliostat field spreads from $X = -24$ m to $X = 24$ m, and is placed at coordinates (40.63 North, 15.38 East), located in Italy, near Naples. A view of the CSP plant with several sun rays traced is shown in Fig. 1; the sun is simulated as a plane surface, placed over the heliostat field, that emits the actual solar DNI along the direction defined by the sun position.

The receiver axis is a line that crosses the center of the heliostat field.

The area occupied by the mirror field is about 1400 m², while the *total reflecting surface* is 584.3 m², thus the *occupation factor* is 0.417.

Due to the aim of this simulation, the DNI values were calculated using the simple model of Hottel [31]. The axis of the

Fig. 1. ¾ view of the CSP plant with reference system and several rays traced; the receiver is on the left top of the figure.

heliostat field is the North-South direction and the target is at South with respect to the field. The beam divergence (the convolution between solar divergence and system imperfections and errors) is defined as a Gaussian enlargement with standard deviation $\sigma = 0.312$ deg [29,30].

The receiver is built as a CPC (Compound Parabolic Concentrator) in conjunction with a cylindrical cavity. The CPC input window is the target of the reflected rays. It has circular shape with radius = 0.5 m; in the reference system its center is placed at (0, −20 m, 30 m). The CPC has acceptance angle = 26 deg (semi-angle) and its output window, coincident with the input window of the cavity, has radius = 0.2192 m; the specular reflectance of its internal surface is set to 0.9 (with 0.1 of absorbance), as the surface of the heliostats. The cylindrical cavity has radius 0.3 m and height 0.2 m; the surface absorbance of the cavity wall is set to 0.6 (the remaining 0.4 is postulated to be Lambertian diffuse reflection). The marginal irradiance is calculated on an annulus with central radius coincident with the radius of the CPC input window and thickness 1/5 of its radius.

5.2. Results

The simulations of the examined CSP plant were performed using the non-sequential simulation software *Lambda Research TracePro*, tracing about 1.2 billion of rays; configuration and input data were set as illustrated in the previous paragraph. The first simulations were performed on the same field (with tower height = 30 m) for different hours of the day (h 9.00 and h 12.00; for h 12.00 the azimuth was approximated always to 0) and three days of the year (day 21 of months June, September and December). The results are summarized in Table 1, where:

– DNI: Direct Normal Irradiance
– avr_cosine: average, among all the heliostats, of the angle cosine between sun rays direction and normal to the heliostat surface
– FIF_MS: Field input flux on the mirroring surface (=DNI * Mirroring Surface)
– FIF_max: Theoretical field input flux on the mirroring surface, taking into account the cosine factor but not the shadowing factor (=DNI * Mirroring Surface * averaged cosine of mirrors with respect to the sun direction)
– FIF_act: actual flux on the mirrors (calculated on the model, it takes into account the shadowing too)
– FOF_max: Theoretical field output flux from the heliostat field (= FIF_act * mirror surface reflectance)
– FOF_act: Actual field output flux from the heliostat field
– FE_MS: Field efficiency based on FIF_MS (=field output flux / FIF_MS)
– FE_max: Field efficiency based on FIF_max (=field output flux / FIF_max)
– FE_act: Field efficiency based on FIF_act (=field output flux / FIF_act)
– CPC input flux: flux that enters into the CPC
– Marg_irradiance: Marginal irradiance on the CPC input window
– CPC direct fract.: fraction of the flux that enters into the CPC and exits without being reflected on its internal surface
– Cavity input flux: flux that enters into the cavity
– Cavity available flux: cavity input flux – reflected flux
– CE_MS: Collection efficiency based on FIF_MS (=available flux / FIF_MS)
– CE_max: Collection efficiency based on FIF_max (=available flux / FIF_max)
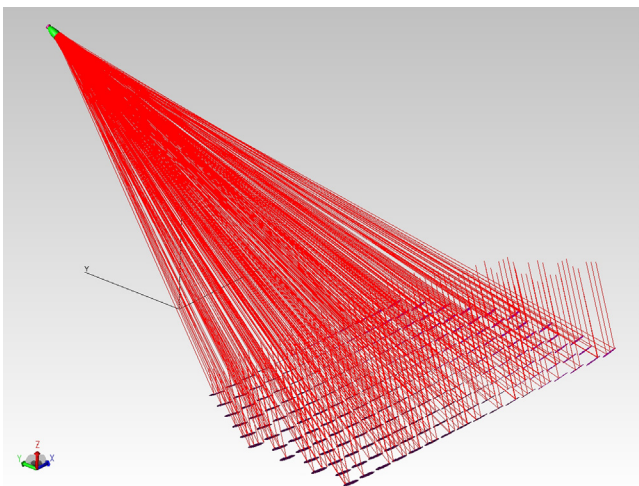– CE_act: Collection efficiency based on FIF_act (=available flux / FIF_act)

Table 1
Results of the mirror field simulations varying sun position and DNI.

Parameter	Jun21 h9	Jun21 h12	Sept21 h9	Sept21 h12	Dec21 h9	Dec21 h12
DNI (kW)	0.793	0.864	0.670	0.797	0.384	0.601
avr_cosine	0.85	0.92	0.90	0.98	0.93	0.99
FIF_MS (kW)	463.4	504.9	391.5	465.7	224.4	351.2
FIF_max (kW)	393.9	464.5	352.4	454.5	209.1	349.1
FIF_act (kW)	394.8	466.0	352.7	456.1	126.0	341.7
FOF_max (kW)	355.3	419.4	317.4	410.5	113.4	307.5
FOF_act (kW)	333.3	389.8	292.9	372.7	109.2	277.0
FE_MS	0.72	0.77	0.75	0.80	0.49	0.79
FE_max	0.85	0.84	0.83	0.82	0.52	0.79
FE_act	0.84	0.84	0.83	0.82	0.87	0.81
CPC input flux (kW)	210.1	251.0	182.9	241.6	70.4	179.2
Marg_Irradiance (kW/m^2)	157.6	183.0	137.8	174.1	50.9	129.2
CPC direct fract.	0.20	0.20	0.20	0.20	0.19	0.20
Cavity input flux (kW)	190.00	227.0	165.3	218.6	63.6	162.1
Cavity available flux (kW)	158.50	189.5	137.9	182.4	53.3	135.2
CE_MS	0.34	0.38	0.35	0.39	0.24	0.38
CE_max	0.40	0.41	0.39	0.40	0.25	0.39
CE_act	0.40	0.41	0.39	0.40	0.42	0.40

Table 2
Results of the mirror field simulations varying the tower height (h) for two sun positions.

Parameter	Jun21 h12.00			Sept21 h9.00		
	$h = 25$m	$h = 30$m	$h = 35$m	$h = 25$m	$h = 30$m	$h = 35$m
DNI (kW)	0.864	0.864	0.864	0.670	0.670	0.670
avr_cosine	0.905	0.920	0.932	0.894	0.900	0.905
FIF_MS (kW)	504.9	504.9	504.9	391.5	391.5	391.5
FIF_max (kW)	456.9	464.5	470.5	350.0	352.4	354.3
FIF_act (kW)	458.4	466.0	472.5	350.9	352.7	354.0
FOF_max (kW)	412.6	419.4	425.3	315.8	317.4	318.6
FOF_act (kW)	362.4	389.8	409.9	275.5	292.9	304.8
FE_MS	0.72	0.77	0.81	0.70	0.75	0.78
FE_max	0.79	0.84	0.87	0.79	0.83	0.86
FE_act	0.79	0.84	0.87	0.79	0.83	0.86
CPC input flux (kW)	241.8	251.0	252.8	179.1	182.9	181.6
Marg_Irradiance (kW/m^2)	166.8	183.0	193.2	128.9	137.8	143.9
CPC direct fract.	0.20	0.20	0.21	0.21	0.20	0.21
Cavity input flux (kW)	216.6	227.0	226.2	160.1	165.3	162.6
Cavity avail. flux (kW)	181.3	189.5	188.6	133.9	137.9	135.6
CE_MS	0.36	0.38	0.37	0.34	0.35	0.35
CE_max	0.40	0.41	0.40	0.38	0.39	0.38
CE_act	0.40	0.41	0.40	0.38	0.39	0.38

Other simulations were performed setting the tower height h at 25 m and 35 m (only for June 21, h 12.00 and September 21, h 9.00); the results are reported in Table 2.

To complete the simulations results numerically presented in Tables 1 and 2, Fig. 2 shows the *irradiance map* on the CPC input window (Jun 21, h 12.00) with the profiles in the X and Y directions of the plot.

5.3. Discussion

The variation of the averaged cosine leads to a difference between FIF_MS and FIF_max variable among the simulations. The difference between FIF_max and FIF_act depends on the shadowing phenomenon (apart from the tolerances on the results), that is considered in FIF_act; in FOF_max the blocking phenomenon is not included, while FOF_act takes it into account. The significance of the utilization of these merit figures emerges from the analysis of FE_MS, FE_max and FE_act. The simulation of Dec 21, h9 reaches the highest value of FE_act, but it is a misguided result: actually, FE_MS is very low, and this means that the plant utilizes the solar radiation in an inefficient way. Moreover, the great difference between FE_max and FE_act proves that the shadowing factor has large influence on the performance for the

configuration Dec 21, h9. It explains the high value of FE_act too: the blocking is very low because the shadowing is high (practically, a large part of radiation that could be blocked does not exist because it does not hit the mirrors due to shadowing). It is confirmed by the difference between FOF_max and FOF_act, that is quite low for Dec 21, h9. It is evident that only the utilization of various optical merit figures permits a sufficiently complete evaluation of the mirror field performance.

The analysis, in the examined case, is less difficult regarding the CPC and the receiver. The value of CPC direct fraction (about 0.2 for all the configurations) indicates that about the 8% of the power that enters into the CPC has to be drained as heat (the 80% of the radiation hits the CPC internal surface, that has 90% of specular reflectance). The Marginal irradiance permits to roughly forecast the effects of radius modifications: if the target radius becomes 0.475 m the target surface difference is 0.07658 m^2 and, considering a *marginal irradiance* of 183 kW/m^2 (Jun 21, h 12), the supposed total flux decreases of 14.0 kW, so it results 237 kW. A direct simulation with target of radius 0.475 m gives the result of 236.7 kW, in perfect agreement with the "supposed total flux", extrapolated from the *marginal irradiance*. This parameter can also be expressed as *marginal linear irradiance* considering the improvement/decrement of flux that depends on the variation of
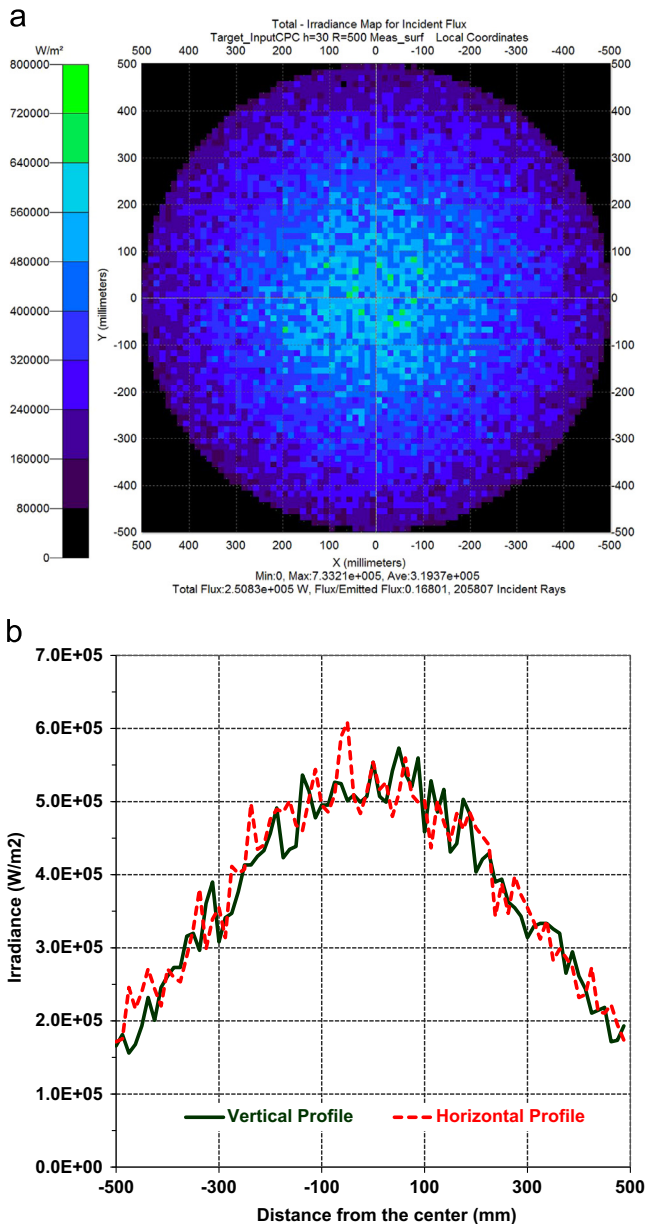
a

b

Fig. 2. Irradiance map on the CPC input window with horizontal and vertical profiles.

Fig. 3. Isocandela plot of all rays (the normal vector is parallel to the CPC axis).

target radius (in the studied case, 575 kW/m). The reflected flux, subtracted from the cavity input flux, leads to the available flux, which is the flux that the designer has to maximize in order to improve the collection efficiency.

In Table 2 the differences that depend from the height of the target are shown for two conditions (Jun 21, h 12 and Sept 21, h 9). The average cosine factor is lower for receiver at 25 m, greater for receiver at 35 m. Moreover, it is conceivable that higher the target is placed, lower will be the blocking; in fact that is demonstrated by the values of FOF_max and FOF_act, that are closer if the tower is higher. As a consequence the highest FE_act is obtained for the target at 35 m. One could expect that in this case also the CE_act is higher, but it does not happen. The reason is that the mean distance of the target from the heliostats increases if it is lifted, thus also the spot dimension increases and the amount of flux that enters into the CPC decreases, as the CPC input flux shows. In particular, this behavior is highlighted by the considerable
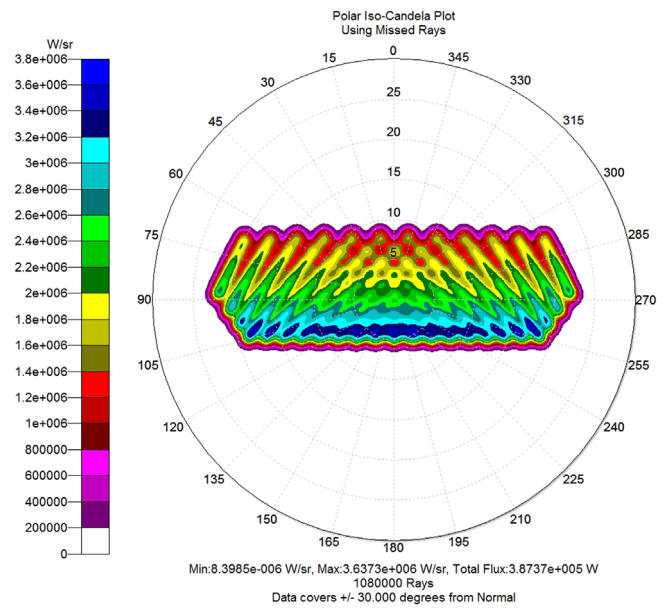
variation of the marginal irradiance, which demonstrates that the spot changes to become larger when the target is lifted.

Another significant and useful graphic output of the software package is the *isocandela plot*: Fig. 3 presents the *isocandela plot* of the rays reflected by the mirrors of the examined field for Jun 21, h12. The acceptance angle of the CPC was set with the help of this map, which immediately shows the intensity distribution referring to the angles between CPC axis and rays reflected by the heliostats.

It evidences an interesting phenomenon: the directions of the rays do not form a symmetrical shape, because the intensity is more concentrated at lower angles (corresponding to the farthest mirrors). For this reason could be a better choice to set the inclination of the CPC (the "0" of the *isocandela plot*) not exactly equal to the direction of the line connecting the center of the heliostat field and the center of the CPC input window in order to increase the *CPC direct fraction*. Really it has to be evaluated the larger spot produced by the farthest mirrors, that leads to more relevant losses and less contribution to the total flux that enters into the CPC for these mirrors. Fig. 4 presents the isocandela plot, for the same simulation as Fig. 3, taking into account only rays that enter into the CPC.

The differences between Figs. 3 and 4 highlight the lower contribution of the farthest mirrors to the flux that enters into the CPC.

Finally the *irradiance maps* of the flux absorbed by the cavity walls (as shown in Fig. 5, referring to the simulation of Jun 21, h 12) are very important in order to facilitate the sizing and the correct choice of the components and to simulate, with other specialized software, the heat transfer to the fluid or, generally, to the medium.

In order to supply to the thermal simulation software a correct input, it is necessary to separate the variations on the map irradiance due to real physical phenomena from the random ones (aroused by the random method that a non-sequential optical simulation software utilizes to perform the simulation). Having fixed the rays number of the simulation, in order to decrease the pixel noise it has to be increased the area of each pixel (by decreasing the pixels number), but also the map resolution decreases. Thus is very useful to determine the best trade-off between map resolution and noise. The best way is to perform at least another simulation with a different "seed" (the starting number for random simulations) and to calculate an averaged
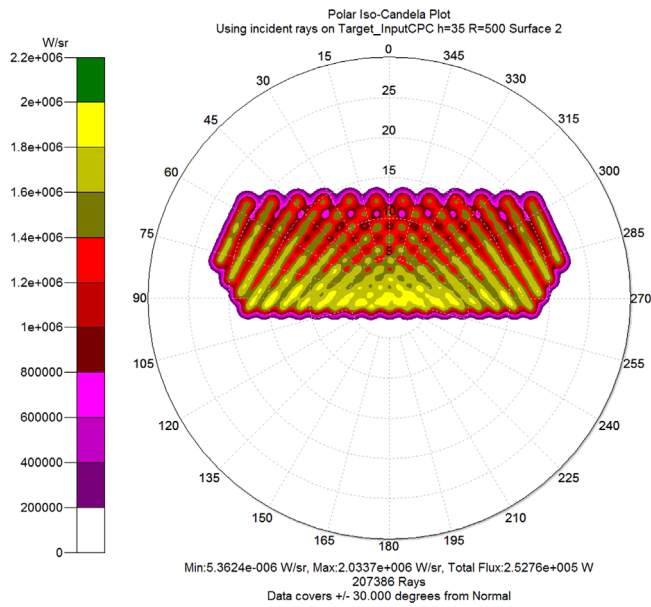
Fig. 4. Isocandela plot of rays that enter into the CPC (normal vector parallel to the CPC axis).
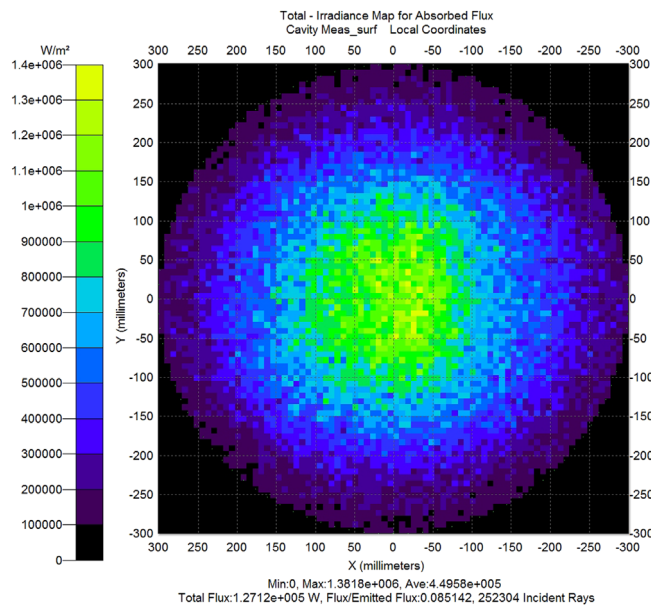

Fig. 5. Absorbed flux of the cavity wall opposite to the input window.

pixel-to-pixel flux difference between the two maps with different seed: in practice, if $P_{1,i}$ is the radiant flux on the i-th pixel of Map_1 and $P_{2,i}$ the radiant flux on the i-th pixel of the Map_2, ABS($P_{1,i}$-$P_{2,i}$)/2 is evaluated[4] for every pixels couple i-th, then the averaged value on all pixels of Map_1 and Map_2 is calculated and divided for the total flux (averaged on the two maps) in order to obtain the Relative Flux Difference. It is an indication of the degree of the random pixel noise, to be compared with the tolerances of the simulations. Due to the fact that there are many pixels per map, even the Relative Flux Difference between only two maps leads to acceptable results. In Fig. 6 the results of this calculation are reported for some couples of maps (every point represents a couple of maps with the same pixels number and different "seed" of the simulation), with increasing pixels number (the total pixels

---

⁴ The division by 2 takes into account that the difference relies to the mean value of the pixel flux.
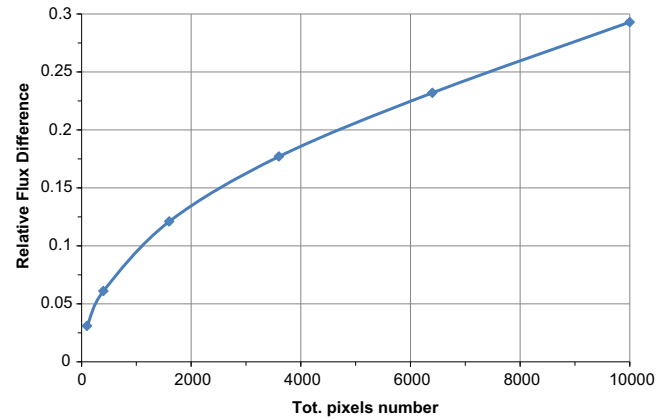

Fig. 6. Variation of the flux due to the randomness of simulations: averaged difference between fluxes on pixels.

number is shown in abscissa, the Relative Flux Difference in ordinate). The rays number is unchanged.

The behavior of the curve is logical (the random noise scales with the squared root of the rays number per pixel, that is roughly proportional to the pixel area), but the values are important: having set the acceptable tolerance for the pixel flux (for example 5%), it is possible to establish the maximum pixels number of the map; a better resolution requests a ray-tracing with a larger rays number.

6. Conclusions

The discussion proposed in this study suggests to utilize a generic non-sequential optical design software to characterize the layout of a mirror field, due to its larger flexibility with respect to dedicated software tools. This flexibility permits to define the best merit figures tailored on the specific study and to compare different configurations of heliostat fields in order to select the more appropriate solution for every solar plant. In this perspective, the most useful optical merit figures for a generic CSP plant were discussed and application criteria were proposed. In particular, it was shown that a deep comprehension of the behavior of a CSP plant (specially concerning the efficiency) requests the utilization of various merit figures at the same time, and it was highlighted the risk of comparing CSP plants only on the basis of a single definition of "efficiency". Specific tests were carried out on a simulated CSP plant in order to verify the effective utility of the discussed optical merit figures. They confirmed the advantages of their introduction and use in the design procedure: suitable merit figures allow to compare the various configurations and to analyze critical components to finally select the optical layout of the CSP plant. The analyzed simulations clearly show the need to utilize multiple optical merit figures at the same time, because by their comparison some important information can emerge. That is due to different "critical parameters" that can be taken into account (land occupation, mirroring surface, tower height and more) in order to evaluate the advantage of a specific configuration. In particular, the simulations evidenced the difference among various ways to evaluate the efficiency of the mirror field, showing the risk of considering only a single merit figure to estimate the optical performance of a CSP plant.

References

[1] Garcia P, Ferriere A, Bezian A-J. Codes for solar flux calculation dedicated to central receiver system applications: a comparative review. Solar Energy 2008;82:189–97.

[2] Yu Qiang, Wang Zhifeng, Xu Ershu. Simulation and analysis of the central cavity receiver's performance of solar thermal power tower plant. Solar Energy 2012;86:164–74.

[3] Varun Prakash R, Bath IK. A figure of merit for evaluating sustainability of renewable energy systems. Renew Sustain Energy Rev 2010;14:1640–3.

[4] Zhang Meimei, Wang Zhifeng, Xu Chao, Jiang Hui. Embodied energy and energy analyses of a concentrating solar power (CSP) system. Energy Policy 2012;42:232–8.

[5] Kumar S. Estimation of design parameters for thermal performance evaluation of box-type solar cooker. Renew Energy 2005;30:1117–26.

[6] Sansoni P, Francini F, Fontani D. Optical characterization of solar concentrator. Opt Laser Eng 2007;45:351–9.

[7] Sansoni P, Fontani D, Francini F, Giannuzzi A, Sani E, Mercatelli L, et al. Optical collection efficiency and orientation of a solar trough medium-power plant installed in Italy. Renew Energy 2011;36:2341–7.

[8] Sansoni P, Francini F, Fontani D, Sani E, Mercatelli L, Jafrancesco D. New strategies and simulation tools to optically design a field of heliostats. Int J Photoenergy 2013;523947:1–7 (Special Issue).

[9] Segal A, Epstein M. Optimized working temperatures of a solar central receiver. Solar Energy 2003;75:503–10.

[10] Segal A, Epstein M. A model for optimization of a heliostat field layout. Proceedings of the 8th International Symposium on Solar Thermal Concentrating Technologies 1996; 989–998.

[11] Segal A, Epstein M. Comparative performances of tower-top and tower-reflector central solar receivers. Solar Energy 1999;65:206–26.

[12] Zaibel R, Dagan E, Karni J, Ries H. An astigmatic corrected target-aligned heliostat for high concentration. Solar Energy Mater Solar Cells 1995;37:191–202.

[13] Riveros-Rosas D, Herrera-Vazquez J, Perez-Rabago CA, Arancibia-Bulnes CA, Vazquez-Montiel S, Sanchez-Gonzalez M, et al. Optical design of a high radiative flux solar furnace for Mexico. Solar Energy 2010;84/5:792–800.

[14] Quaschning V. Technical and economical system comparison of photovoltaic and concentrating solar thermal power systems depending on annual global irradiation. Solar Energy 2004;77:171–8.

[15] Danielli A, Yatir Y, Mor O. Improving the optical efficiency of a concentrated solar power field using a concatenated micro-tower configuration. Solar Energy 2011;85:931–7.

[16] Collado FJ, Guallar J. A review of optimized design layouts for solar power tower plants with *campo* code. Renew Sustain Energy Rev 2013;20:142–54.

[17] Pacheco JE, Reilly HE, Kolb GJ, Tyner CE. Summary of the Solar Two test and Evaluation Program. SAND2000-0372C Technical Report 2000; 1–13.

[18] Collado FJ. Preliminary design of surrounding heliostat fields. Renew Energy 2009;34:1359–63.

[19] Collado FJ. Quick evaluation of the annual heliostat field efficiency. Solar Energy 2008;82:379–84.

[20] Jafrancesco D, Sansoni P, Mercatelli L, Sani E, Fontani D, Francini F, et al. Merit figures for the optical design of CSP plants. J Energy Power Eng 2014 in press.

[21] Welford WT, Winston R. The Optics of Nonimaging Concentrators. 1st ed. New York – San Francisco – London: Academic Press; 1978.

[22] Winston R, et al. Nonimaging optics. Amsterdam: Elsevier Academic Press; 2005.

[23] Almonacid G, Luque A, Molledo G. Photovoltaic static concentrator analysis. Solar Cells 1984;13:163–78.

[24] Brogren M, Nostell P, Karlsson B. Optical efficiency of a PV-thermal hybrid CPC module for high latitudes. Solar Energy 2000;69(Suppl):173–85.

[25] Neber M, Lee H. Design of a high temperature cavity receiver for residential scale concentrated solar power. Energy 2012;47:481–7.

[26] Shuai Yong, Xia Xin-Lin, Tan He-Ping. Radiation performance of dish solar concentrator/cavity receiver system. Solar Energy 2008;82:13–21.

[27] Steinfeld A, Schubnell M. Optimum aperture size and operating temperature of a solar-cavity receiver. Solar Energy 1993;50/1:19–25.

[28] Jafrancesco D, Sansoni P, Francini F, Contento G, Cancro C, Privato C, et al. Mirror array for a solar furnace: optical analysis and simulation results. Renewable Energy 2014;63:263–71.

[29] Harris JA, Duff WS. Focal plane flux distribution produced by solar concentrating reflectors. Solar Energy 1981;27/5:403–11.

[30] Badescu V. Theoretical derivation of heliostat tracking errors distribution. Solar Energy 2008;82:1192–7.

[31] Hottel HC. A simple model for estimating the transmittance of direct solar radiation through clear atmospheres. Solar Energy 1976;18(2):129–34.